



**HAL**  
open science

# Impact of He and H relative depth distributions on the result of sequential He<sup>+</sup> and H<sup>+</sup> ion implantation and annealing in silicon

Nikolay Cherkashin, Nabil Daghbouj, Grégory Seine, Alain Claverie

► **To cite this version:**

Nikolay Cherkashin, Nabil Daghbouj, Grégory Seine, Alain Claverie. Impact of He and H relative depth distributions on the result of sequential He<sup>+</sup> and H<sup>+</sup> ion implantation and annealing in silicon. Journal of Applied Physics, 2018, 123 (16), pp.161556 - 161559. 10.1063/1.5012505 . hal-01736014

**HAL Id: hal-01736014**

**<https://hal.science/hal-01736014v1>**

Submitted on 22 Mar 2018

**HAL** is a multi-disciplinary open access archive for the deposit and dissemination of scientific research documents, whether they are published or not. The documents may come from teaching and research institutions in France or abroad, or from public or private research centers.

L'archive ouverte pluridisciplinaire **HAL**, est destinée au dépôt et à la diffusion de documents scientifiques de niveau recherche, publiés ou non, émanant des établissements d'enseignement et de recherche français ou étrangers, des laboratoires publics ou privés.

# Impact of He and H relative depth distributions on the result of sequential He<sup>+</sup> and H<sup>+</sup> ion implantation and annealing in silicon

N. Cherkashin, N. Daghbouj, G. Seine, and A. Claverie

Citation: *Journal of Applied Physics* **123**, 161556 (2018); doi: 10.1063/1.5012505

View online: <https://doi.org/10.1063/1.5012505>

View Table of Contents: <http://aip.scitation.org/toc/jap/123/16>

Published by the *American Institute of Physics*

---

## Articles you may be interested in

[Tutorial: Junction spectroscopy techniques and deep-level defects in semiconductors](#)

*Journal of Applied Physics* **123**, 161559 (2018); 10.1063/1.5011327

[Effect of the order of He<sup>+</sup> and H<sup>+</sup> ion co-implantation on damage generation and thermal evolution of complexes, platelets, and blisters in silicon](#)

*Journal of Applied Physics* **119**, 135308 (2016); 10.1063/1.4945032

[Self-diffusion in single crystalline silicon nanowires](#)

*Journal of Applied Physics* **123**, 161515 (2018); 10.1063/1.4996987

[Thermodynamic modelling of fast dopant diffusion in Si](#)

*Journal of Applied Physics* **123**, 161527 (2018); 10.1063/1.5001755

[Electrically-inactive phosphorus re-distribution during low temperature annealing](#)

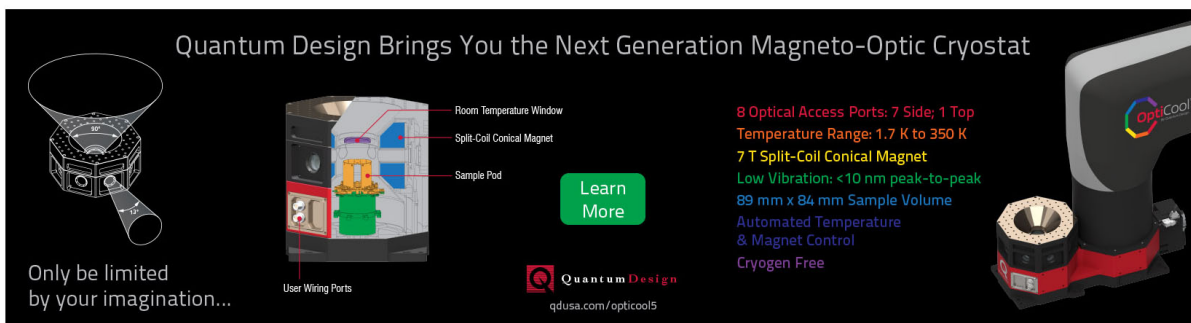
*Journal of Applied Physics* **123**, 161535 (2018); 10.1063/1.5002627

[Blocking germanium diffusion inside silicon dioxide using a co-implanted silicon barrier](#)

*Journal of Applied Physics* **123**, 161540 (2018); 10.1063/1.5002693

---

Quantum Design Brings You the Next Generation Magneto-Optic Cryostat



The advertisement features a central cutaway diagram of the cryostat with labels: Room Temperature Window, Split-Coil Conical Magnet, Sample Pod, and User Wiring Ports. To the left is a 3D perspective view of the device. To the right is a photograph of the physical unit with the 'OptiCool' logo. A 'Learn More' button is positioned in the center. The Quantum Design logo and website URL are at the bottom center.

Only be limited by your imagination...

Learn More

Quantum Design  
qdusa.com/opticool5

8 Optical Access Ports: 7 Side; 1 Top  
Temperature Range: 1.7 K to 350 K  
7 T Split-Coil Conical Magnet  
Low Vibration: <10 nm peak-to-peak  
89 mm x 84 mm Sample Volume  
Automated Temperature & Magnet Control  
Cryogen Free

# Impact of He and H relative depth distributions on the result of sequential He<sup>+</sup> and H<sup>+</sup> ion implantation and annealing in silicon

N. Cherkashin,<sup>a)</sup> N. Daghbouj, G. Seine, and A. Claverie  
 CEMES-CNRS and Université de Toulouse, 29 rue J. Marvig, 31055 Toulouse, France

(Received 6 November 2017; accepted 13 December 2017; published online 3 January 2018)

Sequential He<sup>+</sup>+H<sup>+</sup> ion implantation, being more effective than the sole implantation of H<sup>+</sup> or He<sup>+</sup>, is used by many to transfer thin layers of silicon onto different substrates. However, due to the poor understanding of the basic mechanisms involved in such a process, the implantation parameters to be used for the efficient delamination of a superficial layer are still subject to debate. In this work, by using various experimental techniques, we have studied the influence of the He and H relative depth-distributions imposed by the ion energies onto the result of the sequential implantation and annealing of the same fluence of He and H ions. Analyzing the characteristics of the blister populations observed after annealing and deducing the composition of the gas they contain from FEM simulations, we show that the trapping efficiency of He atoms in platelets and blisters during annealing depends on the behavior of the vacancies generated by the two implants within the H-rich region before and after annealing. Maximum efficiency of the sequential ion implantation is obtained when the H-rich region is able to trap all implanted He ions, while the vacancies it generated are not available to favor the formation of V-rich complexes after implantation then He-filled nano-bubbles after annealing. A technological option is to implant He<sup>+</sup> ions first at such an energy that the damage it generates is located on the deeper side of the H profile.

Published by AIP Publishing. <https://doi.org/10.1063/1.5012505>

## I. INTRODUCTION

Ion implantation of hydrogen and helium is widely used in laboratories and industries to fracture and transfer thin layers of various materials onto different substrates.<sup>1–6</sup> This process, named Smart Cut,<sup>7</sup> is applied to fabricate almost all the Silicon-On-Insulator (SOI) wafers routinely used by the microelectronics and sensor industries. Initially, the process was based on the sole implantation of hydrogen ions at a high fluence followed by bonding and annealing.<sup>7–9</sup> Later, it was realized that the co-implantation of He and H ions could reduce the total fluence needed to fracture silicon by a factor of 3, dramatically reducing fabrication costs.<sup>1,10</sup> However, there has been a debate on the order and the energies under which this sequential implantation should be carried out. For some, H should be implanted first,<sup>1,4,5,11</sup> while for others, He should be first.<sup>12–14</sup> Actually, that controversy only reflected the lack of the understanding of the common physical mechanisms which govern at the atomic scale the efficiency of this synergistic effect.

The basic mechanisms involved in the fracture of heavily hydrogen implanted silicon during annealing are relatively well-known. After ion implantation at room temperature, hydrogen reacts with some of the point defects generated by the collision cascades and form various complexes.<sup>15–17</sup> At the beginning of some low temperature annealing, these complexes evolve and finally form platelets of nanometric dimensions. These platelets are two dimensional discs which result from the co-precipitation of vacancies and hydrogen, with

internal surfaces passivated by hydrogen and internal space filled with H<sub>2</sub> molecules under high pressure.<sup>9,18–20</sup> During annealing, these platelets grow by Ostwald ripening then eventually (if dense enough) coalesce to form nano and micro-cracks (cavities) which, in turn, evolve and fracture the top layer when the surface is covered by some stiffener. When such a stiffener is not bonded on top of the implanted surface, blisters appear on the surface as the result of the local elastic relaxation of the surface layer subjected to the vertical stress exerted by the pressurized cavities. This is why the mechanisms and ingredients involved during the Smart Cut process are often studied and optimized through the study of blister populations at free surfaces.

Agarwal *et al.*<sup>1</sup> were the first to evidence the benefit of using sequential He + H ion implantation. In this pioneering work, it was thought that the main advantage brought by He was that, being chemically inactive, it could segregate more readily into micro-cracks than H. In contrast to H atoms which can bind with silicon atoms and thus not all participate in the pressurization of micro-cracks, the whole He fluence was expected to have contributed to pressurization. For Agarwal *et al.*,<sup>1</sup> the role of H in such a symbiotic process was only limited to the passivation of the internal surfaces of the micro-cracks, the phenomenon which indeed allows a decrease of their energy<sup>17</sup> and, thus promotes the propagation of cracks.<sup>21</sup> Recent investigations have somehow refined this statement.

Indeed, He does react with the vacancies produced during its implantation and can form bubbles which survive even after long time annealing.<sup>19</sup> Actually, both H and He interact with the damage generated by ion implantation and this has an impact on their depth distributions after co-implantation

<sup>a)</sup> Author to whom correspondence should be addressed: nikolay.cherkashin@ceмес.fr

and annealing.<sup>14</sup> The relative contribution of each of these species to the pressurization of micro-cracks observed after annealing has been demonstrated in our previous work.<sup>22</sup> Micro-cracks being formed from the mechanical coalescence of platelets, the synergetic effect shown by the sequential implantation of He and H ions must be resulting from (i) a better efficiency of platelet formation and/or (ii) the maximization of the fractions of He and H fluences involved in the formation and the growth of platelets than of micro-cracks.

In a previous paper,<sup>14</sup> we have studied in detail the influence of the implantation order He + H (He first) or H + He (H first), with He<sup>+</sup> ions being implanted at a deeper depth than H<sup>+</sup> ones, onto the populations of complexes found after such sequential implantations and on how they evolve into platelets, micro-cracks, and eventually nano-bubbles during annealing. This experimental analysis has pointed out the dramatic influence of the “damage,” actually the way the vacancies generated by the two implants are introduced and react with the H and He atoms, on the efficiency of the blistering phenomenon. Finally, we could show and explain that the synergistic effect of sequential He + H implantation is maximized when He is implanted first.

While the influence of the implantation order is understood for He<sup>+</sup> ions being implanted at a deeper depth than H<sup>+</sup> ones, not much is known on the respective energies which should be used to take maximum profit from this sequential ion implantation. For this reason, we have undertaken a detailed study of the effect of the He and H relative depth-distributions, imposed by their respective implantation energies, onto the atomic mechanisms leading to the blistering phenomenon observed after annealing.

## II. EXPERIMENTAL DETAILS AND METHODOLOGY

(001) Si wafers covered by 25 nm-thick thermal SiO<sub>2</sub> layers were implanted at room temperature by He<sup>+</sup> only, H<sup>+</sup> only, or He<sup>+</sup> then H<sup>+</sup> ions (thereafter referenced as “He-alone,” “H-alone,” or “He-first” samples, respectively) with the same nominal fluences of He and H ions, each one of  $1.2 \times 10^{16} \text{ cm}^{-2}$ . H<sup>+</sup> ions were implanted at 10 keV. He<sup>+</sup> ions were implanted at different energies ranging from 28 keV to 5 keV which allowed the He<sup>+</sup> concentration peak to be located deeper, superimposed to, or located shallower than the H<sup>+</sup> concentration peak. Some wafers were alternatively implanted “H-first” for comparison.

Pieces of these wafers were annealed at 350 °C for 3 min, 350 °C for 30 min, or 550 °C for 30 min under nitrogen gas in a conventional oven.

The nominal He and H depth distributions were calculated by SRIM.<sup>23</sup> The cavities buried in the implanted region of the samples and eventually formed during annealing were imaged by optical microscopy. The blisters appearing on the wafer surface were imaged by atomic force microscopy (AFM). The He depth-distributions were measured by secondary ion mass spectroscopy (SIMS). The oxide layer was removed by HF acid prior to the SIMS measurements. Raman spectroscopy was used to detect the various hydrogen related complexes which were formed after implantation. Platelets, nano-bubbles, and micro-cracks were imaged using

appropriate techniques of transmission electron microscopy (TEM).

## III. EXPERIMENTAL RESULTS

### A. Blisters and cavities in samples annealed at 550 °C for 30 min

It is important to note that none of the samples implanted H-only or He-only shows any surface blistering after annealing. Figures 1(a)–1(f) compare the plan-view images obtained by optical microscopy of the samples sequentially implanted “He-first” after annealing at 550 °C for 30 min. The pressurized cavities embedded below the wafer surface and at the origin of the blisters deforming the surface appear through a characteristic phase contrast in the images. Blistering is observed in the samples sequentially implanted at all energies, except for  $E_{\text{He}} = 5 \text{ keV}$  [Fig. 1(f)].

The influence of the He<sup>+</sup> ion implantation energy on the average size and density of the blisters and on the surface fraction they occupy was obtained through the statistical analysis of images such as those shown in Figs. 1(a)–1(e). Results are plotted in Fig. 2.

For the samples sequentially implanted with  $E_{\text{He}} \geq 18 \text{ keV}$ , the blister average diameter of  $1.6 \mu\text{m}$ , the density of  $0.35 \mu\text{m}^{-2}$  and the surface fraction of 80% do not depend on the He<sup>+</sup> ion implantation energy. This suggests that under these conditions, He has been effectively transferred towards the H profile during annealing whatever the initial (positive) distance separating the H and the He profiles.

When the He<sup>+</sup> ion implantation energy decreases to 12 keV and below, down to 8 keV, the blister average diameter continuously decreases down to  $0.8 \mu\text{m}$ , their density increases up to  $0.7 \mu\text{m}^{-2}$  and the surface fraction they occupy

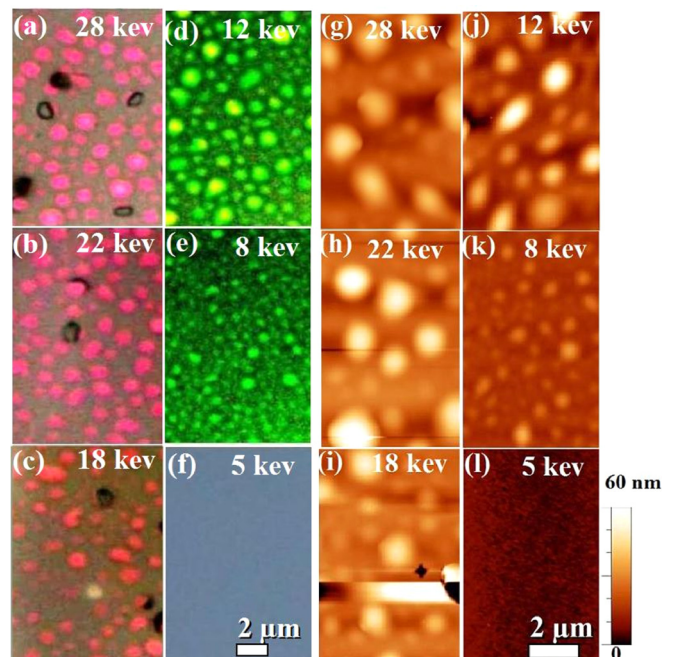


FIG. 1. Optical [(a)–(f)] and AFM [(g)–(l)] images of the samples sequentially implanted He-first with  $E_{\text{He}}$  indicated in the images and annealed at 550 °C for 30 min.



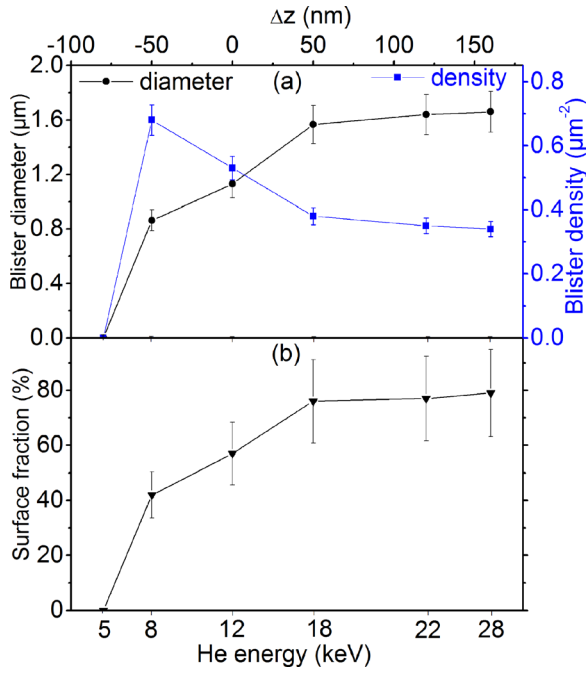


FIG. 2. (a) Average diameter (left axis, black symbols), density (right axis, blue symbols) of the blisters and (b) surface fraction they occupy (black symbols) as a function of He<sup>+</sup> ion implantation energy after He-first sequential implantations and annealing at 550 °C for 30 min.

decreases down to 40%. This might indicate that, when the He profile is shallower than the H one, the portion of implanted He<sup>+</sup> fluence which contributes to the formation of blisters decreases when the distance between the H and the He profiles increases.

In Sec. III B, we check these hypotheses by calculating the densities of H<sub>2</sub> and He molecules which pressurize the populations of blisters we observe.

### B. Densities of molecules pressurizing the populations of blisters

Figure 3 shows the dependence of the blister heights [measured by AFM, Figs. 1(g)–1(k)] on their diameters and this for all samples sequentially implanted with different He<sup>+</sup> ion energies and annealed at 550 °C for 30 min. This graph shows that there is a univocal relationship between the height of a blister and its diameter, regardless of the He<sup>+</sup> ion implantation energy. This characteristic has been noted and discussed in our previous work<sup>22</sup> and results from the fact that all blisters originate from cracks located at the same depth position, where the H concentration is maximum, and that they are all filled with the same gas mixture.

As developed in this previous work,<sup>22</sup> we infer the pressure inside a blister of given diameter and height from the FEM simulation of the elastic deformation generated by some gas pressure inside it. Figure 3 shows the result of such calculations. Interestingly, the variations of internal pressure as a function of blister height are the same as those we have reported in Ref. 22 and for which we could demonstrate that all blisters were filled with about 70% of He and 30% of H<sub>2</sub>.

Following the same methodology, we first calculate the densities of molecules that would be needed to generate the

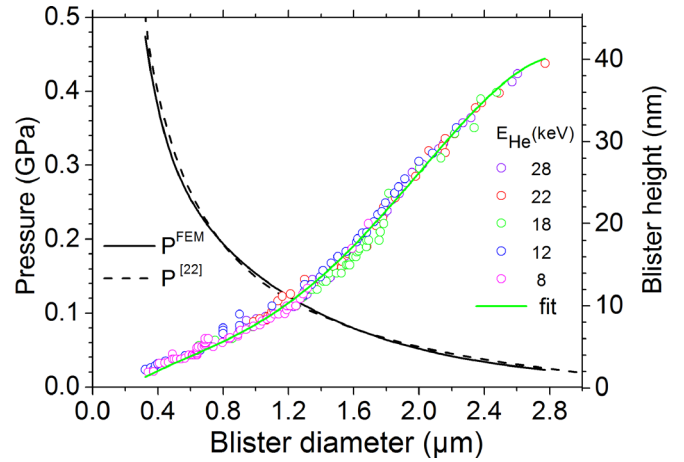


FIG. 3. Height of the blisters (right axis, open circles) and pressure within the blisters (left axis, black solid line) as a function of blister diameters (all samples sequentially implanted with different He<sup>+</sup> ion energies and annealed at 550 °C for 30 min). The black dashed line is a plot of the pressure deduced in Ref. 22 for the blisters filled with 70% of He and 30% of H<sub>2</sub> molecules as a function of their diameters.

observed blisters using exclusively He,  $\rho_{He}$  or H<sub>2</sub>,  $\rho_{H_2}$  molecules.<sup>22</sup> Then, we calculate the areal densities of He molecules,  $\varphi_{He} = x((1-x)\rho_{H_2} + x\rho_{He})$ , and of H<sub>2</sub> molecules,  $\varphi_{H_2} = x\rho_{He} + (1-x)\rho_{H_2} - \varphi_{He}$  contained within the blisters. We also calculate the density of H<sub>2</sub> molecules passivating the internal surfaces of the blisters,  $\varphi_{H_2}^{int.surf}$ . Finally, Fig. 4 shows the calculated values of the fractions of H fluence used for passivating the blisters  $2\varphi_{H_2}^{int.surf}/\Phi_H$ , the fraction of He fluence,  $\varphi_{He}/\Phi_{He}$ , and that of H fluence,  $2\varphi_{H_2}/\Phi_H$  used for pressurizing the observed blisters and this, for the different He ion energies studied here.

The fraction of H fluence used to passivate the internal surfaces of the blisters is proportional to the surface fraction they occupy<sup>22</sup> and thus does not vary much for  $E_{He} \geq 18$  keV but decreases down to 11% when He is implanted at 8 keV. For  $E_{He} = 18$  keV, the blisters contain about 55% and 47% of the implanted He<sup>+</sup> and H<sup>+</sup> fluences, respectively. An increase in He<sup>+</sup> ion energy up to 28 keV has little impact on

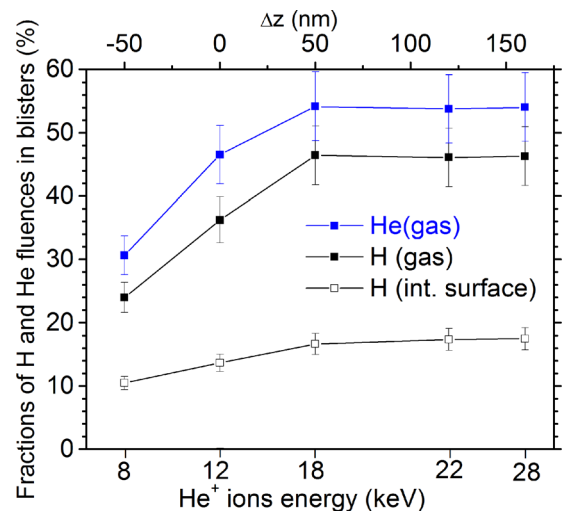


FIG. 4. Fractions of He and H fluences participating in the blister pressurization and passivation as a function of He<sup>+</sup> implantation energy.

those values. Alternatively, when the  $\text{He}^+$  ion energy decreases below 18 keV, the amounts of He and H pressurizing the blisters both decrease.

These results show that the surface fraction that the blisters occupy is directly related to the efficiency of incorporation of He and H molecules into these blisters. When He is implanted deeper than H, He apparently diffuses towards and is finally trapped within the blisters formed in the H-rich region. When He is implanted considerably shallower than H, much less He is involved in the pressurization of the observed blisters. This might be an indication that, in such cases, some He diffuses out of the implanted region during annealing (non-conservative growth) or that it is stored within alternative traps, different from platelets and microcracks.

Sections III C–III F aim at compiling information regarding the mechanisms and ingredients responsible for such behaviors.

### C. H and He depth-distributions after implantation

Figure 5 shows the H and He depth-distributions found in these samples before annealing. Figure 5(a) shows the nominal H depth-distributions introduced by the H implantation step and calculated by SRIM for  $E_H = 10$  keV. SIMS measurements show a quasi-identical profile before annealing. A vertical black dashed line is plotted at the depth having received the maximum damage from this implantation. Figure 5(b) compares: (i) the He profile calculated by SRIM, (ii) the He profile measured by SIMS when He is implanted alone and, (iii) the He profile measured by SIMS after sequential “He-first” implantations, for  $E_{\text{He}} = 18$  keV. The following figures (c), (d), and (e) show the same profiles but after He implantation at 12, 8, and 5 keV, respectively.

Looking at Fig. 5(b), we first notice that the SIMS profile describing the He depth distribution after the implantation of only He is significantly shifted towards the surface in comparison to the profile predicted by SRIM. Interestingly, we note that the He concentration peaks at the depth where the damage introduced by this implantation is maximum [plotted as a vertical olive line in Fig. 5(b)]. Then, we suspect that He diffuses and redistributes during and immediately after implantation and finally get trapped on some of the vacancies generated by the implant. Most interesting is the He profile observed after He-first sequential implantation. The shift of this profile towards even shallower depths only results from the H implantation taking place after He implantation. Thus, this shows that He redistributes at room temperature and gets trapped within the region where H is implanted and most importantly within the region where this H implantation generates some damage (vertical black dotted line).

When the He energy is reduced to 12 keV, the He and H profiles largely overlap. Again, we note that the He SIMS profiles are shifted in comparison to the prediction by SRIM. After He only implantation, the He profile again peaks at the depth where the damage is maximum. Further H implantation (He-first) leads to some slight redistribution of the He atoms and the shift of the profile peak towards larger depths.

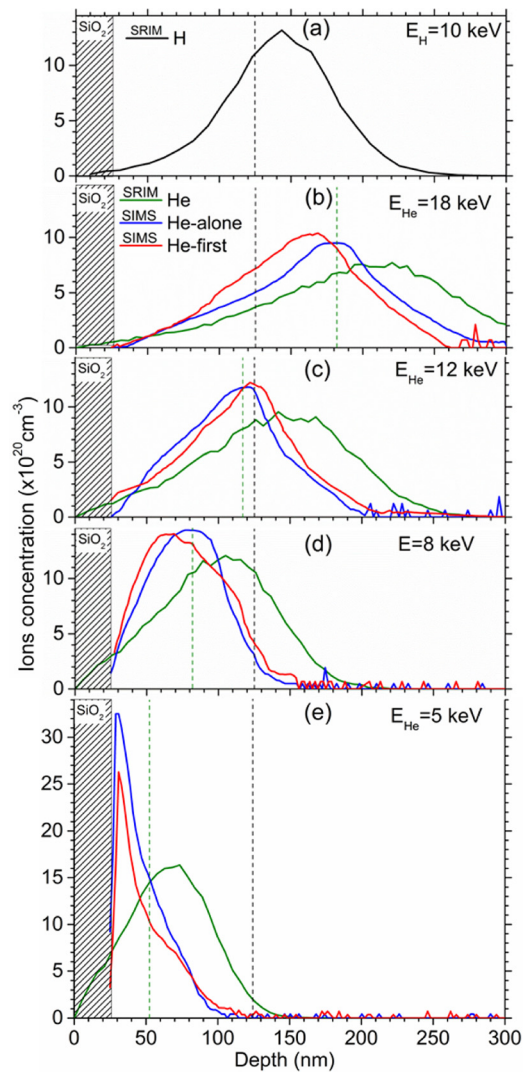


FIG. 5. (a) H and [(b)–(e)] He depth distributions calculated by SRIM (H: black line, He: olive line) and measured by SIMS (He-alone: blue line, He-first: red line) for  $E_H = 10$  keV (a) and  $E_{\text{He}} = 18$  keV (b), 12 keV (c), 8 keV (d) and 5 keV (e). The vertical black dashed and olive line identify the positions of the damage peak concentrations calculated by SRIM for  $\text{H}^+$  and  $\text{He}^+$  ion implantations, respectively.

Interestingly, we note that the damage peak generated by the H implant is this time located deeper than the one generated by the He implant. We again evidence that He redistributes towards the damage generated by the second (H) implant during or immediately after this implant.

When the He energy is reduced down to 8 keV [Fig. 5(d)], we note that He redistributes after implantation and is again trapped in the region where the induced damage is maximum. However, this time the H profile which is subsequently implanted only marginally overlaps with the initial He profile. Moreover, the damage generated by this H implant is principally located deeper than the He implant. In this case, the He atoms redistribute after H implantation, in small part towards the damage generated by the H implant (see the shoulder visible on the deep side of the red profile at depths of about 100–120 nm) but for a larger part towards the surface.

Finally, when He is implanted at 5 keV, the He profile is dramatically shifted towards the surface where it accumulates. This shows that the  $\text{SiO}_2/\text{Si}$  interface acts as a trap for

He. This trap is far more attractive than the damage generated by the He implant. Moreover, after subsequent H implantation, some of this He gets trapped in the region where some damage was generated by the H and He implants (see the shoulder visible on the deep side of the red profile at depths of about 50–100 nm).

To summarize, we have evidenced that, in general, He tends to redistribute during and after implantation and gets trapped in the region where the damage, Is and Vs, is generated by this implant. When H is implanted after He (He-first), He redistributes during or after this H implant and tends to get trapped in the region where this additive damage is generated. However, this redistribution occurs only when the H implantation and profiles significantly overlap with the previously implanted He profile. If not, and in particular, when the He profile is implanted much shallower than the H profile, then the SiO<sub>2</sub>/Si interface acts itself as a trap and favors He accumulation close to this interface.

#### D. Hydrogen complexes formed after implantation

H<sup>+</sup> ion implantation and further reactions with the vacancies generated by this or any other implantation result in the formation of a large variety of characteristic H complexes which are now well identified.<sup>15–17</sup> In the following, we compare the populations of complexes formed after He-first sequential He + H implantations to those generated by a H-only implantation and eventually to those generated by a H-first sequential implantation. In other words, we focus our attention onto the impact of the He<sup>+</sup> implantation, before H<sup>+</sup> implantation, onto the distribution of H atoms within these various complexes, and this as a function of He<sup>+</sup> energy, i.e., as a function of the distance between the He and H depth profiles.

Figure 6 shows the Raman spectra obtained on the H-only and He + H co-implanted samples.

The black spectrum in Fig. 6(a) shows the well-known signatures of the main complexes formed after H<sup>+</sup> implantation in silicon. This typical spectrum shows several characteristic signatures in the low frequency range (LF,  $\lambda < 2050 \text{ cm}^{-1}$ ) which correspond to multi-vacancy hydrogenated complexes V<sub>n</sub>H<sub>m</sub> ( $n \geq m$ ) and IH<sub>2</sub> and in the high frequency range (HF,  $\lambda > 2050 \text{ cm}^{-1}$ ) which correspond to multi-hydrogen hydrogenated complexes such as VH<sub>3</sub>, VH<sub>4</sub>, and V<sub>2</sub>H<sub>6</sub>.<sup>14–16</sup> These H-rich complexes are known to be the precursors of the famous platelets which form during annealing and are at the origin of blistering and fracture.<sup>14,16</sup> Note that the Si(001)-H complexes, characteristic of the passivation of the internal surfaces of these platelets, are not detected. Thus, after such an implantation, the H atoms are distributed in some proportions among these different complexes, as reflected by the amplitudes of their different signatures.

When He is implanted after this H implantation (H-first) at 18 keV, i.e., deeper than the H implant, this distribution obviously changes, more V-rich complexes are formed but the H-rich complexes have almost disappeared. Two important conclusions can be drawn from these observations. First, the second (He) implant has provided the silicon crystal with extra-vacancies (originating from the Frenkel pairs) which

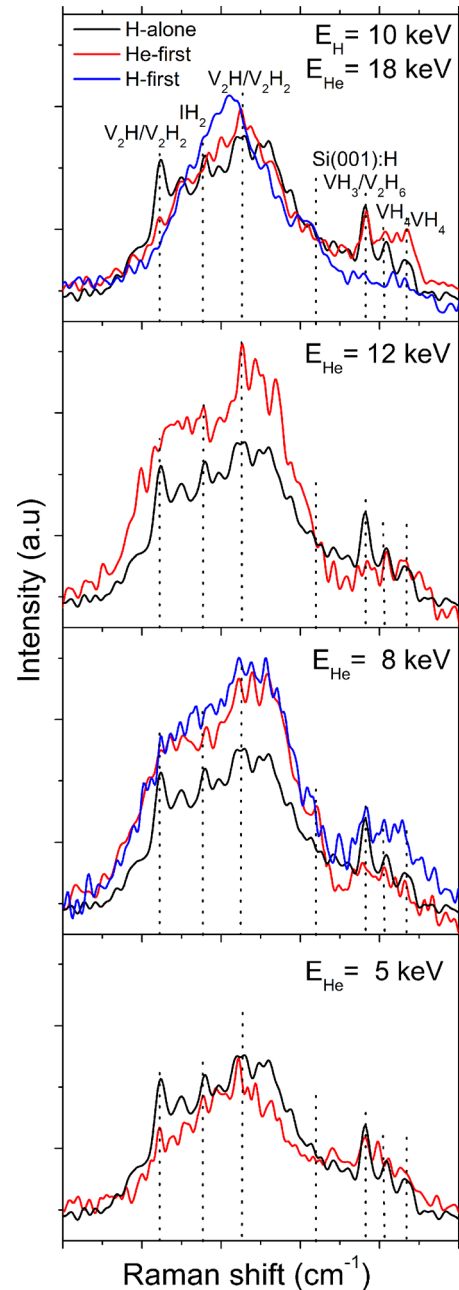


FIG. 6. Raman spectra obtained from the samples implanted with H alone (black line) and co-implanted He-first (red line) and H-first (blue line) at  $E_{\text{He}}$  of 18 keV (a); 12 keV (b); 8 keV (c) and 5 keV (d), before annealing.

have reacted with the already present H atoms. Second, the initially present H-rich complexes must have been ballistically destroyed, then the H atoms redistributed through recoil events by this second implant. Finally, following the second implant, the H atoms, interstitials, and vacancies diffuse and are distributed in new proportions to form these different complexes. Alternatively, when H is implanted after the He implant (He-first), the population of all these complexes is almost the same as when H is implanted alone, with only more VH<sub>4</sub> complexes. Overall, there are fewer vacancies involved in these complexes than in those observed after H-first implantation. This is a clear indication that the vacancies initially generated by this first He<sup>+</sup> implantation are not “available” to react later with H when H is finally implanted.



This may occur because of only two reasons: (i) they have recombined with Is and annihilated in large proportion during and after implantation and/or (ii), they are formed too deep, too far from the H-rich region, and instead cluster in the form of multi-vacancies or nano-bubbles filled with He, two mechanisms that would not be favorable in presence of H, as the result obtained on the H-first sample shows.

Figure 6(b) shows the spectrum we obtain when He is implanted first at an energy of 12 keV, i.e., when the He and H profiles largely overlap. In this case, we note a large increase of the signal associated with the V-rich complexes and the decrease of those associated with the  $\text{VH}_3$  and  $\text{V}_2\text{H}_6$  defects. The system becomes more V-rich as compared to the 18 keV case. This is an indication that some of the vacancies initially created by the first He implant were this time partly redistributed and rendered available to form H complexes after the second implant. Thus, they had not all annihilated within the H-rich region as it was previously suggested after the analysis of the 18 keV He-first implantation. Instead, it suggests that when they cannot incorporate into a H complex, these vacancies cluster and may form a tank able to store He atoms.

Figure 6(c) compares the results obtained when  $\text{He}^+$  ions are implanted in both orders at 8 keV. We note that both sequential implantations give rise to almost the same spectra in the low frequency range with many more V-rich and I-rich complexes than in the H-alone sample. This is because, as observed in the case of the 12 keV implantation, the damage generated by the He implant can interact with the implanted H atoms. Moreover, the signals corresponding to the  $\text{V}_2\text{H}_6$  and  $\text{VH}_4$  complexes are stronger in the H-first sample than in the He-first one. The signal corresponding to the  $\text{VH}_4$  complexes is even stronger after H-first sequential implantation than after H-only implantation. These last observations show that part of the V-rich complexes generated by the H implant can be fragmented by the second He implantation then the H atoms they contain are redistributed and incorporated into H-rich complexes. Keeping in mind that the transfer of kinetic energy between He ions and complexes can only result in the recoil of H atoms preferably in the forward direction (towards larger depths), it is very probable that, in such samples, the H-rich complexes found in the H-first sample are located deeper than the V-rich complexes.

Finally, Fig. 6(d) shows the spectra obtained when He is implanted at such a low energy that the two profiles are spatially well separated. In such a case, the spectra obtained for He-first and H-first (not shown) samples are identical and resemble very much to that obtained for H-only implantation. In other words, the damage generated by He implantation cannot interact with H atoms and complexes.

There are a couple of very important conclusions that can be extracted from this set of experiments. First, we evidence that the type and concentration of the different complexes that can be observed after sequential  $\text{He} + \text{H}$  implantation dramatically depend on the order but also on the ion energies during both H and He implantations. When H is implanted first, the vacancies generated by the subsequent He implantation can interact with the H complexes already present in the Si lattice. This tends to favor the

formation of V-rich hydrogen complexes, at the expense of the H-rich complexes. Alternatively, when He is implanted first, the vacancies and interstitials migrate until they mostly recombine, partially form multi-vacancy clusters which can host He molecules. If H is then implanted, the populations of complexes which are formed will depend on whether or not these vacancies will be redistributed by the second (H) implant and will contribute to the formation of complexes. When He is implanted significantly deeper than H, these vacancies are located too deep and cannot contribute to the final complexes formed within the H-rich region. The population of complexes is about the same as the one observed after H-only implantation. When the He energy is reduced, the vacancies generated by this implant can be redistributed and used to form H complexes after the H implant. This results in the formation of large quantities of V-rich hydrogen complexes. When the He energy is further reduced, the vacancies generated by the He implant are located out of the H profile and cannot contribute to the formation of H complexes.

### E. Platelets, bubbles, and micro-cracks after annealing

Figure 7 shows a selection of bright-field cross-sectional (110) TEM images obtained on these samples.

In the sample implanted at  $E_{\text{He}}$  of 18 keV [Fig. 7(a)], one observes a narrow band of micro-cracks mostly parallel to the (001) wafer surface. The band of defects is about 50 nm-wide and centered at a 140 nm distance from the wafer surface, i.e., at the depth where H precipitates during annealing.<sup>22</sup>

The sample sequentially implanted at  $E_{\text{He}}$  of 8 keV [Fig. 7(b)] also contains a single band of defects roughly located at the same depth but spread over a much wider region (65 nm-thick) and of much smaller sizes (typically of 100 nm).

The sample sequentially implanted with He at 5 keV [Fig. 7(c)] contains two well-separated bands of defects. The first one is centered at the depth of about 140 nm where the H concentration is maximum and contains nano-cracks with diameters smaller than 50 nm. The second band is about 40–50 nm-wide and centered at a distance of 50 nm from the wafer surface. It contains He nano-bubbles only [marked by arrows in the inset of Fig. 7(c)] depth distributed over a distance of about 30 nm.

### F. He depth distribution in annealed samples

We now look at the characteristics of He redistribution during annealing of these samples (Fig. 8). As is well-known, they are two main artifacts affecting SIMS measurements of He and H implanted samples after annealing. First, the amplitude of the signal, i.e., the concentration of He may be dramatically underestimated when probing a region containing gas filled cavities. Second, the depth position of the micro-cracks can be underestimated since sputtering of the material during SIMS experiment should result in a continuous increase of blister heights as micro-cracks approach the wafer surface,<sup>22</sup> and thus, the conversion of sputtering time into depth may be elusive in practice. Thus, these spectra should be used as “fingerprints” only to reveal qualitative information.



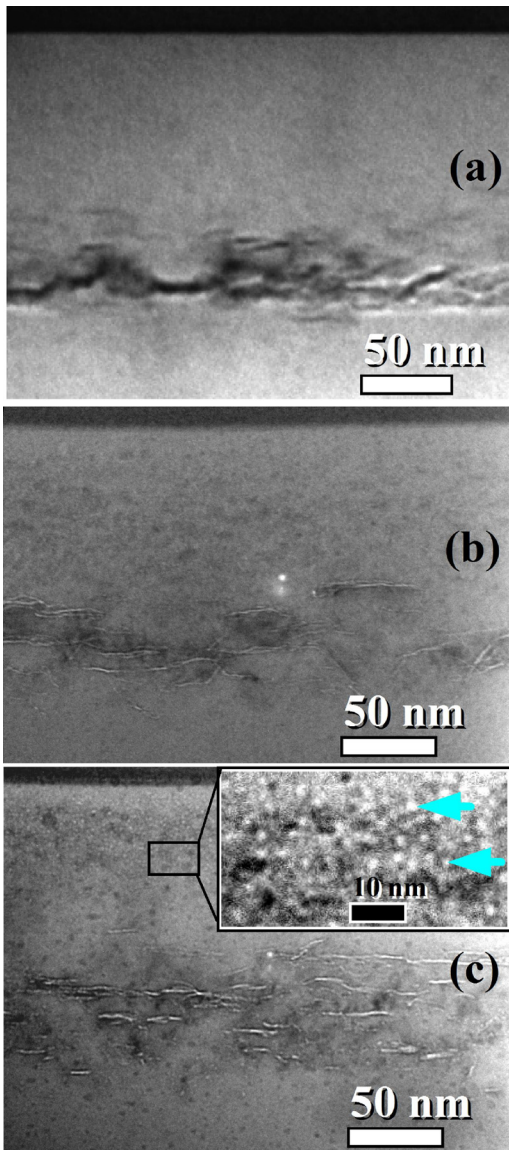


FIG. 7. Bright-field cross-sectional (110) TEM images taken in off-Bragg and defocused conditions of the samples sequentially implanted He-first at  $E_{\text{He}}$  of 18 keV (a); 8 keV (b) and 5 keV (c), and annealed at 550 °C for 30 min. The arrows in the inset of (c) show the He-related nano-bubbles.

Figure 8(a) compares the He profiles obtained before and after annealing at 550 °C for 30 min for the sample sequentially implanted “He-first” with He ion energy of 18 keV. After annealing, He has been massively redistributed and shows the concentration peak characteristic of He precipitation in the region where the gas-filled nano-cracks and platelets were detected by TEM.

Figure 8(b) shows the evolution of the He concentration profile within the sample sequentially implanted with He at 8 keV when it is annealed at 350 °C for 3 min, for 30 min, or at 550 °C for 30 min. As previously discussed, the as-implanted profile is already asymmetric and shows a concentration peak located at a 60 nm distance from the wafer surface and a shoulder located 60 nm deeper. Annealing at 350 °C for 3 min gives rise to a redistribution of He within two Gaussian-like profiles, one 90 nm-wide and centered at a depth of 70 nm and a second one, 50 nm-wide and centered

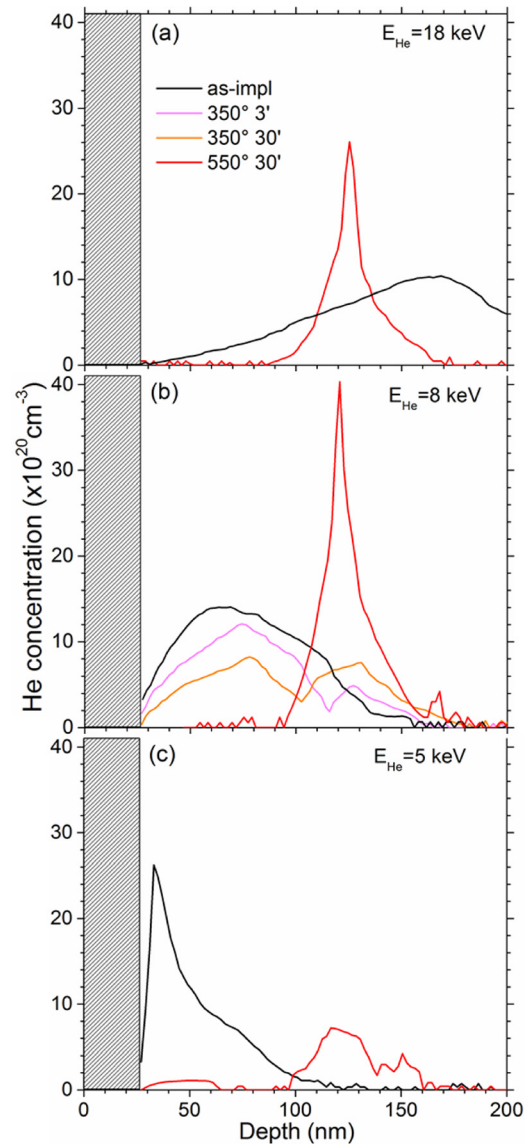


FIG. 8. SIMS measurements of the He concentration profiles before and after annealing in the samples sequentially implanted He-first at  $E_{\text{He}}$  of 18 keV (a); 8 keV (b) and 5 KeV (c).

at a depth of 130 nm. It is worth noting that these distributions are exactly centered on the depth positions of the damage peaks calculated by SRIM for these two implantations (see Fig. 5).

Increasing the annealing time up to 30 min results in the progressive transfer of He from the shallow profile towards the deepest one. This suggests that initially two types of traps, well spatially separated, exist for hosting He, and that the traps located deeper are more stable than those found close to the surface. Finally, annealing at 550 °C for 30 min leads to the total redistribution of He towards the deepest trapping region where TEM reveals the presence of nano-cracks.

Figure 8(c) shows the results obtained after annealing of the sample sequentially implanted with He at 5 keV. The as-implanted sample shows an asymmetric shape with a concentration peak located close to the  $\text{SiO}_2/\text{Si}$  interface and a shoulder located at a 70 nm distance from the wafer surface.

After annealing at 550 °C for 30 min, He has not massively but only partly redistributed towards the H-rich region. Instead, we still observe two distinct, spatially separated, regions hosting He, at about the same depths as previously observed but after less energetic annealing. This shows that when the two damaged regions generated by the two implantations do not overlap, He cannot be easily trapped deeper than it was implanted. We also have to note the considerable loss (about 60%) of the implanted He fluence resulting from such annealing. This fluence loss, which was not so clearly evidenced for larger He energies, shows that when He<sup>+</sup> ions are implanted shallower than the H<sup>+</sup> ones, He can diffuse easily towards the wafer surface. This obviously results in a non-conservative evolution of the system during annealing.

#### IV. DISCUSSION AND CONCLUSIONS

There are a number of important facts which have been established along this study.

The first one concerns He diffusion. We have evidenced that He diffuses a lot at room temperature after sole and sequential implantations. First, it redistributes on its own damage formed during its implantation, then may further diffuse towards the damage generated by the second H implant if they overlap. We believe that this evidences the high diffusivity of He even at room temperature and its ability to be trapped by larger multi-vacancy complexes.

By studying the hydrogen complexes formed after implantation, we have evidenced that the type and concentration of the various complexes which are formed depend on the availability of the vacancies generated by the two implants. When H is implanted first, the vacancies generated by the second He implantation may interact with the H complexes already present in the Si lattice. This tends to favor the formation of V-rich complexes at the expense of the H-rich ones. When He is implanted first, it is likely that more vacancies and Si interstitials annihilate than when He is implanted through H complexes. Moreover, these vacancies are stabilized in the form of multi-vacancy clusters stable at room temperature and are located at the depth where the damage is maximum. The effect of the second H implantation will depend on whether or not the damage it generates is located deep enough to destabilize these clusters and render the single vacancies they are composed of available to the system to form the H complexes. If yes, then V-rich complexes will massively form. This is clearly observed when He is implanted at more or less the same depth as H. Alternatively, when He is implanted much deeper than H, the vacancies left by the He implant after annihilation will not be redistributed to the system. When the He is implanted much shallower than H, the vacancies generated by the first implant, although possibly fragmented by the H implantation, are well separated from those generated by the H implant and thus cannot diffuse to and interact with H.

The combination of characterization results obtained on the annealed samples shows that when He is implanted sufficiently deeper than H, so that its maximum damage and associated vacancies also located deeper than the H implant, then He can diffuse towards the depth where H precipitates

forming platelets and micro-cracks. In such a case, about half of the He and H implanted fluences participate in the pressurization of the blisters. The rest of the implanted fluences is most likely stored within the platelets distributed around the micro-cracks. When the He energy is such that its damage profile is shallower than that generated by the H implant, two trapping regions exist, each one centered on the depth position of the damage profiles generated by the implantations. The traps generated by the He implantation ultimately appear as nano-bubbles while those located deeper are the classical platelets known to host H and eventually He. Depending on the distance between these two damage profiles and on the overlapping of the vacancy populations they generate, He will be able or not to diffuse from the less stable (the nano-bubbles) to the more stable (the H passivated platelets and nano-cracks) defects during annealing. Moreover, when He<sup>+</sup> ions are implanted much shallower than the H<sup>+</sup> ones, He can diffuse easily towards the wafer surface where it can escape or be trapped. In such a case, the thermal evolution of the system becomes non-conservative and as a result of such a competitive redistribution of He between nano-bubbles, platelets and the wafer surface, only one third of the implanted He and H fluences finally participates in the formation and pressurization of blisters.

In summary, by studying the influence of the relative positions of H and He implants on the blistering efficiency, we have enlightened the role played by the damage, more specifically the vacancies, generated by the two implantations onto the effect of some He + H sequential implantation. At room temperature and during annealing, He diffuses easily in and towards the vacancy rich regions. To favor blistering, He should be able to diffuse to the H-rich region, while the vacancies generated by its implantation should not be rendered available after the second implant to form H complexes. If one defines the efficiency of the process as the ability to store as much as possible of the implanted fluence within the blisters, optimized technological options for the use of sequential He + H implantation will be obtained by implanting He first at an energy such that the damage profile is located on the deeper side of the H profile.

<sup>1</sup>A. Agarwal, T. E. Haynes, V. C. Venezia, O. W. Holland, and D. J. Eaglesham, *Appl. Phys. Lett.* **72**(9), 1086 (1998).

<sup>2</sup>C. Qian and B. Terreault, *J. Appl. Phys.* **90**, 5152 (2001).

<sup>3</sup>O. Moutanabbir and B. Terreault, *Appl. Phys. Lett.* **86**, 051906 (2005).

<sup>4</sup>S. Reboh, F. Schaurich, A. Declémy, J. F. Barbot, M. F. Beaufort, N. Cherkashin, and P. F. P. Fichtner, *J. Appl. Phys.* **108**, 023502 (2010).

<sup>5</sup>C. Lagahe-Blanchard, N. Soubie, S. Sartori, H. Moriceau, A. Soubie, B. Aspar, P. Nguyen, and B. Blondeau, *Electrochem. Soc. Symp. Proc. PV2003-19*, 346 (2003).

<sup>6</sup>I. Radu, I. Szafraniak, R. Scholz, M. Alexe, and U. Gösele, *J. Appl. Phys.* **94**, 7820 (2003).

<sup>7</sup>M. Bruel, *Electron. Lett.* **31**, 1201 (1995).

<sup>8</sup>M. Bruel, *Nucl. Instrum. Methods B* **108**, 313 (1996).

<sup>9</sup>J. Grisolia, G. Ben Assayag, A. Claverie, B. Aspar, C. Lagahe, and L. Laanab, *Appl. Phys. Lett.* **76**, 852 (2000).

<sup>10</sup>M. K. Weldon, M. Collot, Y. J. Chabal, V. C. Venezia, A. Agarwal, T. E. Haynes, D. J. Eaglesham, S. B. Christman, and E. E. Chaban, *Appl. Phys. Lett.* **73**(25), 3721 (1998).

<sup>11</sup>X. Duo, W. Liu, M. Zhang, L. Wang, C. Lin, M. Okuyama, M. Noda, W.-Y. Cheung, S. P. Wong, P. K. Chu, P. Hu, S. X. Wang, and L. M. Wang, *J. Appl. Phys.* **90**(8), 3780 (2001).

- <sup>12</sup>P. Nguyen, K. K. Bourdelle, T. Maurice, N. Sousbie, A. Boussagol, X. Hebras, L. Portigliatti, F. Letertre, A. Tauzin, and N. Rochat, *J. Appl. Phys.* **101**, 033506 (2007).
- <sup>13</sup>O. Moutanabbir, B. Terreault, M. Chicoine, F. Schiettekatte, and P. J. Simpson, *Phys. Rev. B* **75**, 075201 (2007).
- <sup>14</sup>N. Daghbouj, N. Cherkashin, F.-X. Darras, V. Paillard, M. Fnaiech, and A. Claverie, *J. Appl. Phys.* **119**, 135308 (2016).
- <sup>15</sup>O. Moutanabbir and B. Terreault, *J. Chem. Phys.* **121**, 7973 (2004).
- <sup>16</sup>S. Personnic, K. K. Bourdelle, F. Letertre, A. Tauzin, N. Cherkashin, A. Claverie, R. Fortunier, and H. Klocker, *J. Appl. Phys.* **103**, 023508 (2008).
- <sup>17</sup>N. Cherkashin, F.-X. Darras, P. Pochet, S. Reboh, N. Ratel-Ramond, and A. Claverie, *Acta Mater.* **99**, 187–195 (2015).
- <sup>18</sup>J. Grisolia, F. Cristiano, G. Ben Assayag, and A. Claverie, *Nucl. Instrum. Methods Phys. Res., Sect. B* **178**, 160 (2001).
- <sup>19</sup>X. Hebras, P. Nguyen, K. K. Bourdelle, F. Letertre, N. Cherkashin, and A. Claverie, *NIMB* **262**, 24 (2007).
- <sup>20</sup>N. Cherkashin and A. Claverie, “Characterization of process-induced defects,” in *TEM in Micro-Nanoelectronics*, edited by A. Claverie (Wiley, 2012), pp. 165–193. ISBN: 9781848213678.
- <sup>21</sup>S. Reboh, J. F. Barbot, M. F. Beaufort, and P. F. P. Fichtner, *Appl. Phys. Lett.* **96**, 031907 (2010).
- <sup>22</sup>N. Cherkashin, N. Daghbouj, F.-X. Darras, M. Fnaiech, and A. Claverie, *J. Appl. Phys.* **118**, 245301 (2015).
- <sup>23</sup>J. F. Ziegler and J. P. Biersack, See <http://www.srim.org> for SRIM computer code.